University of Pennsylvania
**ScholarlyCommons**

Departmental Papers (Chemistry)                    Department of Chemistry

# Molecular Recognition of Ketamine by a Subset of Olfactory G Protein–coupled Receptors

Jianghai Ho

Jose Manuel Perez Aguilar
*University of Pennsylvania*, perezagu@sas.upenn.edu

Lu Gao

Jeffery G. Saven
*University of Pennsylvania*, saven@sas.upenn.edu

Hiroaki Matsunami

*See next page for additional authors*

Follow this and additional works at: http://repository.upenn.edu/chemistry_papers

Part of the Biochemistry Commons, Organic Chemistry Commons, and the Physical Chemistry Commons

## Recommended Citation

# Molecular Recognition of Ketamine by a Subset of Olfactory G Protein–coupled Receptors

## Abstract

Ketamine elicits various neuropharmacological effects, including sedation, analgesia, general anesthesia, and antidepressant activity. Through an in vitro screen, we identified four mouse olfactory receptors (ORs) that responded to ketamine. In addition to their presence in the olfactory epithelium, these G protein (heterotrimeric guanine nucleotide–binding protein)–coupled receptors (GPCRs) are distributed throughout the central nervous system. To better understand the molecular basis of the interactions between ketamine and ORs, we used sequence comparison and molecular modeling to design mutations that (i) increased, reduced, or abolished ketamine responsiveness in responding receptors, and (ii) rendered non-responding receptors responsive to ketamine. We showed that olfactory sensory neurons (OSNs) that expressed distinct ORs responded to ketamine in vivo, suggesting that ORs may serve as functional targets for ketamine. The ability to both abolish and introduce responsiveness to ketamine in GPCRs enabled us to identify and confirm distinct interaction loci in the binding site, which suggested a signature ketamine-binding pocket that may guide exploration of additional receptors for this general anesthetic drug.

## Disciplines

Biochemistry | Organic Chemistry | Physical Chemistry

## Author(s)

Jianghai Ho, Jose Manuel Perez Aguilar, Lu Gao, Jeffery G. Saven, Hiroaki Matsunami, and Roderic G. Eckenhoff

# Molecular recognition of ketamine by a subset of olfactory G protein–coupled receptors

**Jianghai Ho**[#1], **Jose Manuel Perez-Aguilar**[#2,†], **Lu Gao**[#2], **Jeffery G. Saven**[2], **Hiroaki Matsunami**[1,3], and **Roderic G. Eckenhoff**[4,‡]

[1]Department of Molecular Genetics and Microbiology, and Department of Neurobiology, Duke University, Durham, NC 27710, USA.

[2]Department of Chemistry, University of Pennsylvania, Philadelphia, PA 19104, USA.

[3]Duke Institute for Brain Sciences, Duke University, Durham, NC 27710, USA.

[4]Department of Anesthesiology and Critical Care, Perelman School of Medicine, University of Pennsylvania, Philadelphia, PA 19104, USA.

[#] These authors contributed equally to this work.

## Abstract

Ketamine elicits various neuropharmacological effects, including sedation, analgesia, general anesthesia, and antidepressant activity. Through an in vitro screen, we identified four mouse olfactory receptors (ORs) that responded to ketamine. In addition to their presence in the olfactory epithelium, these G protein (heterotrimeric guanine nucleotide–binding protein)–coupled receptors (GPCRs) are distributed throughout the central nervous system. To better understand the molecular basis of the interactions between ketamine and ORs, we used sequence comparison and molecular modeling to design mutations that (i) increased, reduced, or abolished ketamine responsiveness in responding receptors, and (ii) rendered non-responding receptors responsive to ketamine. We showed that olfactory sensory neurons (OSNs) that expressed distinct ORs responded to ketamine in vivo, suggesting that ORs may serve as functional targets for ketamine. The ability to both abolish and introduce responsiveness to ketamine in GPCRs enabled us to identify and confirm distinct interaction loci in the binding site, which suggested a signature ketamine-binding pocket that may guide exploration of additional receptors for this general anesthetic drug.

## INTRODUCTION

Despite the widespread use of general anesthetics, the targets underlying their actions remain poorly defined. This is especially true for the small, relatively featureless inhaled anesthetics, but also for the more potent injectable anesthetics, such as the barbiturates and alkylphenols. For example, evidence suggests that the injectable general anesthetics propofol and etomidate serve as co-agonists of the inhibitory cys-loop ligand-gated ion channels (LGICs), such as $\gamma$-aminobutyric acid receptor type A ($GABA_A$) and glycine receptors (1). However, these receptors are neither necessary nor sufficient for the general anesthetic action of these drugs (1), indicating that other targets must exist. Unfortunately, the heavy emphasis on LGICs has marginalized the search for other targets. That other targets can subserve general anesthesia is exemplified by the injectable drug ketamine, which does not have effects on the LGICs, but rather is thought to act by antagonizing *N*-methyl-D-aspartate (NMDA) receptors (1). In addition to being a general anesthetic, ketamine has distinct effects in vivo, including dysphoria, hallucinations, and analgesia. Other more specific NMDA antagonists do not share this wide range of properties in vivo, and thus, it is generally recognized, although little explored, that ketamine has other molecular targets that might transduce or contribute to its general anesthetic effects. Indeed, ketamine has antidepressant activity (2), raising the possibility that it interacts in the central nervous system (CNS) with heterotrimeric guanine nucleotide–binding protein (G protein)–coupled receptors (GPCRs), a receptor superfamily frequently targeted by antidepressants and other psychotherapeutics (3–5). This possibility is consistent with the demonstration that ketamine binds to opioid and muscarinic receptors (6).

GPCRs are the largest class of druggable receptors, yet they have been little explored as transducing components of general anesthesia. We have previously shown that the inhalational anesthetic halothane binds to the prototypical class A GPCR, rhodopsin, and competitively inhibits retinal binding (7). Olfactory receptors (ORs) are the largest group of GPCRs (8). It is generally thought that only a single OR-encoding gene is expressed in each olfactory sensory neuron (OSN) (8) and that each OR is "tuned" to recognize a limited repertoire of generally small, volatile molecules (9). The ~1000 different murine and ~300 human ORs monogenically expressed across the olfactory epithelium (8) enable olfactory stimuli to generate and transmit unique activation patterns to the olfactory cortex, allowing humans to discriminate large numbers of olfactory stimuli (10). Using dissociated OSNs, we previously demonstrated that volatile anesthetics do indeed activate individual OSNs, and in a highly selective manner (11). Moreover, evidence has emerged that ORs are distributed widely in the CNS (12) and also in various tissues around the body, not just the olfactory epithelium. For example, ORs in the gut (13) and the testicles (14, 15) appear to subserve very specific signaling roles in the regulation of normal physiology and development. Thus, it is plausible that selective anesthetic activation renders ORs as candidate mediators for some of the CNS actions that anesthetics exhibit.

To identify previously uncharacterized anesthetic targets and to better understand the structural features underlying molecular recognition of a general anesthetic such as ketamine, we screened a set of mouse ORs and found that ketamine activated a very limited repertoire of these ORs at physiologically relevant concentrations. Then, through a

combination of molecular modeling and mutagenesis, we defined key ketamine recognition elements in the binding site of these class A GPCRs, which enabled predictive modulation of the anesthetic response.

## RESULTS

### In vitro screen for ketamine-responsive ORs

To identify ORs that are activated by ketamine, we screened 51 broadly distributed and previously characterized murine ORs (table S1) (16) with a cyclic adenosine 3′,5′-monophosphate (cAMP)–mediated luciferase reporter assay to measure receptor activity (17). In the primary screen, we stimulated Hana3A cells with 100 μM ketamine and selected 12 candidate responsive ORs for a secondary screen, where responses to ketamine were measured in triplicate and compared to those of cells treated with solvent as a negative control. We found that MOR136-1 and MOR139-1 responded significantly ($P$   0.05) and specifically to ketamine among the tested anesthetics ( Fig. 1, A and B). This screen was subsequently repeated with 21 ORs that are members of the MOR136, MOR139, or related OR families (table S2), and another OR, MOR136-3, was identified that also responded significantly and specifically to ketamine (Fig. 1A), but not to other anesthetics (Fig. 1B). We constructed dose-response curves of the responders MOR136-1, MOR139-1, and MOR136-3, which responded to ketamine in a concentration-dependent manner (Fig. 1C) with half-maximal effective concentration ($EC_{50}$) values that approximate the steady-state plasma concentrations of ketamine present during anesthesia in the mouse (18).

### Comparative homology modeling of ORs and ketamine-docking calculations

To understand the structural basis of ketamine recognition by the murine ORs MOR136-1, MOR136-3, and MOR139-1, we generated comparative (homology) models of MOR136-1 and other ORs (Fig. 2A). These approximate structural models provided a vehicle for generating hypotheses regarding binding site residues that could be tested by site-directed mutagenesis (19). Models were constructed on the basis of available GPCR structures, including bovine rhodopsin (20), human $\beta_2$ adrenergic receptor ($\beta_2$AR) (21), turkey $\beta_1$AR (22), human $A_{2A}$ adenosine receptor (23), and human $D_3$ dopamine receptor (24), which, when combined, constituted five templates used to generate the OR models (fig. S1). For each of the murine OR sequences, 100 models were generated with the Modeller software (25, 26) (see Materials and Methods). The best structure based on Modeller's scoring function was selected in each case. Each model structure contained the canonical seven transmembrane (TM) helices connected by intracellular and extracellular loops and the small helical segment at the C terminus, which is nearly perpendicular to the seven-helix bundle (27–29). We chose to focus mainly on the structure of the ketamine responder MOR136-1 and its putative binding pocket (Fig. 2). Through computational docking studies, we identified a ligand-binding site that is consistent with that previously identified for ORs (30) (Fig. 2A, yellow atoms). In addition, we also generated models of MOR136-1 based on the structures of the activated states of bovine rhodopsin (31) and the human $\beta_2$AR (32, 33). The representative models of the inactive and active conformations were compared and displayed a backbone coordinate root mean square deviation (RMSD) of 2.3 Å for the seven TM helices (TM1 to TM7) and the adjacent perpendicular helix (H8) (fig. S2). For

comparison, the backbone RMSD is 2.5 Å for these protein segments (TM1-TM7-H8) between the inactive (2RH1.pdb) and active (3SN6.pdb) crystallographic structures of the human $\beta_2$AR (21, 32). Furthermore, conformations and orientations of ketamine in the binding site of the active receptor (which are known as docking poses) were comparable to those observed in the model structure generated with inactive structures.

With the representative comparative models, docking calculations for R-ketamine were performed with AutoDock4 (34), and a binding site for R-ketamine in MOR136-1 was identified (Fig. 2A). In the case of MOR136-1, the three best-scoring docking results are located at the same binding site, which largely comprised side chains from helices TM3, TM5, and TM6 (Fig. 2, B to D). With these three ketamine-docked structures, residues having an atom within 5.0 Å of any atom of ketamine were identified as potential lining residues of the ketamine-binding pocket in MOR136-1, yielding 16 lining residues (Fig. 2, A and E). In addition, camphor, an odorant containing the same cyclohexanone moiety as ketamine and that activates the ketamine responder MOR136-1 (16), was also docked to the model of MOR136-1. This ligand bound to the same binding site as did ketamine and also displayed similar binding interactions (fig. S3A).

## Structural analysis of the ketamine-binding site

Comparison of the amino acid residues at the 16 binding site positions suggests possible key interactions relevant to the activation of MOR136-1 by ketamine. The ketamine pose 1 (Fig. 2B) has the positively charged ammonium nitrogen in close proximity to Ser105$^{3.33}$ (3.9 Å to the hydroxyl oxygen) and Asp109$^{3.37}$ (4.5 Å to the carboxyl oxygen). Superscripts on residues indicate the location within the GPCR structure according to the Ballesteros-Weinstein indexing system (35). For example, Asp109$^{3.37}$ refers to the aspartic acid residue with amino acid residue number 109 in the MOR136-1 sequence, whereas 3.37 refers to the 37th position on the 3rd TM helix. The 37th position is defined relative to the most conserved residue at each TM helix, which is assigned to the 50th position (Fig. 2E, blue letters). In the ketamine pose 2 (Fig. 2C), proximity to Ser105$^{3.33}$ is again observed between the ketone oxygen atom of ketamine and the hydroxyl oxygen atom of Ser105$^{3.33}$, with a distance of 3.2 Å. The structure also suggests a possible role of Ser112$^{3.40}$ because of the proximity of its hydroxyl oxygen to the ketamine ammonium nitrogen (distance of 3.8 Å; Fig. 2C). Last, in pose 3 (Fig. 2D), the ketone oxygen atom of ketamine is close to the hydroxyl oxygen atom of Ser112$^{3.40}$, with a distance of 4.6 Å, whereas its Cl atom is 4.5 Å from the hydroxyl oxygen atom of Thr279$^{7.42}$ (Fig. 2D). The potential importance of the position occupied by Ser112$^{3.40}$ in receptor-ligand binding was suggested from studies of the murine eugenol OR, mOR-EG, in which the equivalent position (Ser113$^{3.40}$) forms a hydrogen bond with the eugenol ketone group (36). Camphor also elicits a response in heterologous cells expressing MOR136-1 (16). In our model structure, the ketone oxygen atom of camphor is positioned 3.4 Å from the hydroxyl oxygen atom of Ser112$^{3.40}$, which is similar to the interaction observed in one of the docked poses of ketamine (Fig. 2D and fig. S3A).

To test the sensitivity of the docking results to the model structure, we generated an additional model of MOR136-1 from structures of the active forms of related GPCRs as

mentioned earlier, and this model was used for docking calculations involving ketamine. Through a similar procedure, the same set of key binding site residues within 5.0 Å of the ligand were identified (fig. S3B). Various poses were observed in the binding site, and we observed interactions similar to those seen when using the inactive-based structure. In pose 1, the ketone oxygen atom of ketamine is 3.2 Å from the hydroxyl oxygen atom of Ser112$^{3.40}$, whereas in pose 2, the ammonium nitrogen atom of ketamine establishes interactions with this residue (3.1 Å; see fig. S3B). These results are consistent with the interactions observed in the poses of ketamine and camphor in the OR models based on inactive structures (Fig. 2 and fig. S3A). These comparative models, however, likely have neither the fidelity nor the resolution to distinguish between subtleties in the binding of ketamine to the active and inactive forms of the receptor.

In initial screens, only MOR136-1 and MOR136-3 among the MOR136 family of receptors responded to ketamine (fig. S4). Among the identified binding site residues, the only position that differs between MOR136-1 and MOR136-3 is position 3.37 (Asp109$^{3.37}$ in MOR136-1) (Table 1). This observation suggests that the different responses of these two receptors to ketamine may be a result of the different residues at this position. Henceforth, amino acid residue numbers corresponding to those of MOR136-1 are used unless otherwise indicated.

Receptor sequence comparisons, particularly at the proposed binding site positions, can potentially be useful in understanding the features that distinguish responders from nonresponders (Table 1). Focusing on positions in the putative binding pocket, a combination of residues was identified that could potentially distinguish responders from nonresponders. The TM3 helix seems to have the role of a structural hub that delimits the ketamine-binding site, and analysis of the positions in this helix provided insights about the particular function of the different amino acid residues in the binding of ketamine. For example, at position 105$^{3.33}$, the ketamine-responsive receptors contained either a Ser or a Thr, but these polar residues were much less frequent at this position among the nonresponsive receptors, all but one of which have hydrophobic residues at this position. All of the responders have a Phe at position 104$^{3.32}$, an Ala at 108$^{3.36}$, and a Ser at 112$^{3.40}$. Thus, informed by the screening results, molecular models, and sequence comparison, two classes of mutations were considered to further explore the details of OR activation by ketamine: mutations were identified that were expected to (i) decrease the ketamine responsiveness of MOR136-1 and (ii) convert the nonresponders MOR136-4 and MOR136-11 into ketamine-responsive receptors.

**Decreasing the ketamine responsiveness of MOR136-1**

From inspection of the model structures and the comparison of the sequences of responders and nonresponders, three residues were identified as potentially playing important roles in ketamine binding by MOR136-1: Ser105$^{3.33}$, Asp109$^{3.37}$, and Ser112$^{3.40}$. Mutations to these residues were expected to decrease the ketamine responsiveness of the receptor. As suggested by the docking studies, the hydroxyl group of Ser105$^{3.33}$ may coordinate the ammonium group or the ketone group of ketamine, and the mutation S105A$^{3.33}$ would remove this interaction. Similarly, the negatively charged Asp109$^{3.37}$ might electrostatically

associate with the positively charged ammonium group of ketamine; thus, the mutation D109A$^{3.37}$ would be expected to abrogate this interaction. Ser112$^{3.40}$ is present in all responders and may form polar interactions with the ketone or the ammonium groups of ketamine. Thus, the mutation S112A$^{3.40}$ would eliminate this hydrogen bonding interaction. To explore the effect of multiple such mutations, the double mutant (S105A$^{3.37}$/S112A$^{3.40}$) and the triple mutant (S105A$^{3.33}$/D109A$^{3.37}$/S112A$^{3.40}$) were also considered. Furthermore, we proposed the mutation D109S$^{3.37}$ for MOR136-1 to introduce the amino acid residue present in MOR136-3 (one of the other responders); this mutation was expected to decrease the response to ketamine, consistent with the initial screen (Fig. 1A).

We performed site-directed mutagenesis of MOR136-1, measured responses to ketamine, and constructed dose-response curves for each mutant (Fig. 3A). As predicted, the S105A$^{3.33}$ mutant decreased the response to ketamine. Similarly, S112A$^{3.40}$ was expected to attenuate the ketamine response, and this mutation completely eliminated the response. Consistent with the single point mutation results, the double mutant S105A$^{3.33}$/S112A$^{3.40}$ also completely eliminated responsiveness to ketamine (Fig. 3A). However, the mutation D109A$^{3.37}$ unexpectedly enhanced the response of the mutant receptor to ketamine when compared to that of the wild-type receptor. Furthermore, the triple mutant S105A$^{3.33}$/D109A$^{3.37}$/S112A$^{3.40}$ displayed a ketamine response that was comparable with that of the single mutant S105A$^{3.33}$. Thus, the D109A$^{3.37}$ mutation appears to be an enhancing mutation, which rescued some of the effects introduced by the S105A$^{3.33}$ and S112A$^{3.40}$ mutations (Fig. 3A).

We further explored the sensitivity of the receptor response to the size and hydrophobicity of the amino acid residue at this particular position (109$^{3.37}$) by producing the single-site mutants D109N$^{3.37}$, D109L$^{3.37}$, D109S$^{3.37}$, D109K$^{3.37}$, and D109V$^{3.37}$. Despite their different physicochemical nature, the D109N$^{3.37}$ and D109L$^{3.37}$ mutants exhibited responses to ketamine that were similar to that of the wild-type receptor (D109$^{3.37}$) (Fig. 3B); the D109S$^{3.37}$ mutant receptor exhibited a slight enhancement in the sensitivity of its response to ketamine. Introducing either a β-branched side chain (D109V$^{3.37}$) or a large, positively charged side chain (D109K$^{3.37}$) at this position eliminated the response of the mutant receptor to ketamine (Fig. 3B). Given that Asn, Leu, and Asp have similar molecular volumes and flexible side chains, these observations are consistent with steric (van der Waals) interactions between the protein and ketamine determining the response, with smaller amino acids (serine) yielding a greater normalized response.

To investigate the conformational elements associated with the role of position 109$^{3.37}$ in ketamine binding, constrained molecular dynamics (MD) simulations were performed in the wild-type MOR136-1 receptor (fig. S5), and solvent-accessible surface areas and volumes of the putative binding pockets were calculated (table S3). The variability of the conformations adopted by the Asp109$^{3.37}$ side chain was clearly reflected in the superposition of different snapshots from the entire 100-ns trajectory (fig. S5A). The Asp109$^{3.37}$ side chain was observed to take on various conformational states, a fraction of which overlapped with the putative ketamine-binding site.

For mutations that resulted in a decreased response, the possibility that the mutation caused protein misfolding and trafficking dysfunction was also considered. We used fluorescence-activated cell sorting (FACS) to analyze the cell surface expression of the receptors and found that both the S112A$^{3.40}$ and S105A$^{3.33}$/S112A$^{3.40}$ mutants were similarly abundant at the surface of transfected human embryonic kidney (HEK) cells (fig. S6), which suggests that the proteins had passed cellular quality control mechanisms, an indication of correct folding. Thus, the diminished responses of these mutant receptors to ketamine are likely a result of direct modulation of receptor-ketamine interactions.

## Introducing ketamine responsiveness to MOR136-4 and MOR136-11

Introducing a mutation that renders a receptor responsive is perhaps a more stringent test of our understanding of ketamine recognition than is reducing or eliminating a response. Among the 16 identified binding pocket residues, 2 nonresponders, MOR136-4 and MOR136-11, were similar to MOR136-1 (Table 1). MOR136-4 displays a high degree of similarity with the responder MOR136-1: 12 of the 16 residues in the binding pocket are identical. The docking calculation and the sequence comparison analysis suggested that positions 104$^{3.32}$, 105$^{3.33}$, and 112$^{3.40}$ might be responsible for the difference in the ketamine responses of MOR136-1 and MOR136-4.

MOR136-4 is the only receptor in the MOR136 family that has a Tyr instead of a Phe at position 104$^{3.32}$, which is located in TM3 and is near to the extracellular entrance to the binding pocket. MOR136-4 also does not have a polar residue at position 105$^{3.33}$. At position 112$^{3.40}$, a Ser residue is conserved in the responding GPCRs, but the larger, polar Asn residue is present at this position in MOR136-4. In addition, position 207$^{5.47}$ in TM5 of MOR136-4 differs from that in MOR136-1 (I207$^{5.47}$), with MOR136-4 being the sole receptor in the MOR136 family that has the polar Thr residue instead of Ile at this position. For MOR136-4, we therefore proposed and generated the mutations Y104F$^{3.32}$, I105S$^{3.33}$, N112S$^{3.40}$, and T207I$^{5.47}$ to test our hypotheses that each of these four residues plays an important role in ketamine binding and, if involved, that these proposed mutations would introduce or increase ketamine responsiveness of the mutant MOR136-4 receptor. MOR136-11 shows less overall sequence identity with MOR136-1, with 11 of 16 residues in the identified binding pocket being identical (Table 1). We hypothesized that the TM3 mutations I105S$^{3.33}$ and G108A$^{3.36}$ would introduce ketamine responsiveness to the nonresponder MOR136-11. Another mutation, G108V$^{3.36}$, enabled us to test the role of the size of the side chain at position 108$^{3.36}$. We performed site-directed mutagenesis as described earlier, measured receptor responses to ketamine, and found that N112S$^{3.40}$, designed to mimic the identity of the binding site of MOR136-1, introduced ketamine responsiveness to MOR136-4; however, the other two mutations, I105S$^{3.33}$ and T207I$^{5.47}$, failed to introduce ketamine responsiveness. The mutation Y104F$^{3.32}$ at the entry to the binding pocket resulted in a degree of ketamine responsiveness that was even greater than that of wild-type MOR136-1 (Fig. 4A).

To further investigate the role of position 104$^{3.32}$, we introduced the opposite mutation, F104Y$^{3.32}$, in the responder MOR136-1, a mutation that rendered the receptor nonresponsive (fig. S7). To understand the molecular basis for the importance of position

$104^{3.32}$, we performed constrained MD simulations of both wild-type MOR136-4 and its $Y104F^{3.32}$ mutant (fig. S8 and see Materials and Methods). The trajectory of the wild-type receptor showed that $Tyr104^{3.32}$ and $Thr279^{7.42}$ formed a side-chain hydrogen bond (fig. S8, A and C), highly restricting the conformations available to the side chain of Tyr. In contrast, because $Phe104^{3.32}$ could not form side-chain hydrogen bonds with $Thr279^{7.42}$, it was less constrained and explored a wider range of side-chain conformations, better accommodating ketamine (fig. S8B). This mutation also yields a large reduction in the solvent-accessible surface area and the volume of the putative binding pocket (table S3).

We also performed FACS analysis of cells expressing the MOR136-4 mutants (fig. S9) and found that the hyperactive MOR136-4 $Y104F^{3.32}$ mutant had the least cell surface abundance of all of the mutants, demonstrating that all of the mutants were expressed on the cell surface to some degree and that there was little or no correlation between the amount of cell surface receptor and the extent of its response to ketamine.

A similar procedure was repeated to obtain the dose-response curves for each mutant of MOR136-11 (Fig. 4B). The $G108A^{3.36}$ mutation did not result in ketamine responsiveness, but the $G108V^{3.36}$ mutation did to a modest degree. The $I105S^{3.33}$ mutation did not result in substantially increased ketamine sensitivity; however, the double mutation $I105S^{3.33}/$ $G108A^{3.36}$ introduced a modest ketamine response to MOR136-11. We also performed FACS analysis of cells expressing MOR136-11 mutants (fig. S10) and found that all of the mutants, except for $G108A^{3.36}$, were present on the cell surface.

## Elucidating the signature elements for the ketamine-binding site

The general behavior of the binding site positions that we investigated displayed particular features (Fig. 5A). At positions $105^{3.33}$ and $112^{3.40}$ in TM3, the small polar residues Ser and Thr were present in ketamine responders. At position $108^{3.36}$, the small apolar side chains of Ala or Val are preferred. The presence of a Phe residue at position $104^{3.32}$ was necessary to confer ketamine responsiveness to MOR136-1. Position $104^{3.32}$ is located at the extracellular entrance of the binding pocket, but also appeared to modulate pocket sterics. At position $109^{3.37}$, the presence of the negatively charged Asp residue was not essential; indeed, its replacement by the small residues Ala or Gly substantially improved ketamine responsiveness (Fig. 5A and Table 2). In addition, MOR136-5, a natural variant with Gly at $109^{3.37}$, also responded to ketamine (Fig. 5B and see Discussion).

In the context of the GPCR structure, the location of the putative ketamine-binding site based on the docking results is consistent with binding site residues identified in other ORs (30, 36–39). Additionally, when the proposed ketamine poses in the TM region of the OR are compared with other ligand-receptor structures of different class A GPCRs found in the CNS, a similar pattern of interacting residues is observed (fig. S11A). Moreover, the deep penetration of ketamine in the TM bundle (as evidenced mainly by contact with positions 3.40 and 5.47) is comparable to that observed in complexes of muscarinic receptors with tiotropium and iperoxo, and in a complex of a histamine receptor with doxepin, which display the deepest ligand penetration of class A GPCRs (40).

**In vivo responses of OSNs to ketamine**

Because our experiments thus far were performed in an in vitro heterologous cell expression system, we sought to demonstrate the in vivo activation of MOR136-1 by ketamine. Thus, we stimulated the mouse olfactory epithelium by intranasal application of ketamine solutions and then performed fluorescence in situ hybridization (FISH) analysis for ORs to identify OSNs expressing specific ORs, as well as immunohistochemical analysis of phosphorylated ribosomal protein S6 (pS6) as a marker of OSN activation (Fig. 6, A to C) (41–43). When we examined the activation of OSNs labeled with the MOR136-1 full-length copy RNA (cRNA) probe, we observed that 6.6% of labeled OSNs were activated when exposed to phosphate-buffered saline (PBS), whereas 17, 24, and 25% of OSNs labeled with the MOR136-1 cRNA probe were activated by 3, 30, and 300 μM ketamine, respectively (Fig. 6D). This result was in contrast to that from experiments with a control OR, MOR171-2 (commonly known as M71)–labeled OSNs, in which fewer than 4.2% exhibited activation under any condition (Fig. 6D).

# DISCUSSION

Ketamine, a relatively potent general anesthetic, analgesic, and antidepressant, is generally considered to transduce its hypnotic properties through interactions with NMDA receptors (1). Here, we provide evidence for a highly specific interaction of ketamine with ORs, which suggests that a component of ketamine's pleiotropic actions may result from interactions with these or other GPCRs in the CNS. The analgesic action of ketamine, for example, might result from specific actions on opioid GPCRs, whereas its antidepressant effects could arise from interactions with monoaminergic GPCRs. Beyond providing evidence of other potential GPCR actions, it is possible that specific interactions between ketamine and ORs in the CNS may be responsible for some of its actions. Analyses of human RNA sequencing (RNASeq) data from the Illumina BodyMap project, as well as other database resources, provided evidence that ORs may be expressed in various tissues throughout the body and that they are not limited to the olfactory epithelium (12, 44). Although it is unclear whether these "ectopic" ORs are functionally expressed in these tissues, or what their function might be, these findings may indicate broader functions for ORs in chemosensation that are not limited to smell.

In addition to suggesting relevant molecular targets of ketamine, our combined experimental and modeling study provides a molecular-level view of the GPCR elements that are involved in ketamine binding, as well as their spatial distribution in the binding pocket. The location of the putative ketamine-binding pocket in the TM region is consistent with sites previously identified in other ORs (30, 36–39). Our docking studies of ketamine in MOR136-1 (Fig. 2C), followed by mutational validation, indicates the importance of hydrogen bonding for ketamine responsiveness (Table 2). Moreover, the features of the identified ketamine-binding site are substantiated by an analysis of ligand contacts of different class A GPCRs found in the CNS (fig. S11). We note that no structural information about these other receptor complexes was used in the computational modeling of the OR structures. Although we were unable to distinguish differences in ketamine contacts between active and inactive OR structures, it is noteworthy that the relative position of ketamine in the OR is very

similar to that of the $M_2R$-iperoxo complex, which represents a GPCR in its active state conformation (fig. S11B).

In addition to polar elements, we also were able to validate the importance of steric features in the OR ketamine site. For example, of the 16 candidate binding pocket residues, the 2 responders from the MOR136 family (MOR136-1 and MOR136-3) differ only at site $109^{3.37}$ (Table 1), and mutations at this position helped us understand the different responses of these two receptors to ketamine. Three categories of mutations were identified relative to the wild-type receptor: (i) the mutations $D109A^{3.37}$ and $D109S^{3.37}$ increased the sensitivity of the receptor to ketamine; (ii) the mutations $D109N^{3.37}$ and $D109L^{3.37}$ yielded receptors with ketamine responsiveness comparable to that of the wild-type receptor; and (iii) the mutations $D109V^{3.37}$ and $D109K^{3.37}$ eliminated ketamine responsiveness. We interpret these results by suggesting that a small nonpolar residue better accommodates ketamine in the binding pocket. Further, the valine residue ($D109V^{3.37}$) could disrupt the transmembrane helix segment (TM3), whereas the lysine residue ($D109K^{3.37}$) might result in the formation of a salt bridge to $Glu111^{3.39}$ on TM3 or simply bring the bulky, positively charged $Lys109^{3.37}$ into the binding pocket. In either case, the fit with ketamine becomes less favorable.

To understand these steric features better, we performed constrained MD simulations with MOR136-1. On the basis of the results from the MD simulations of MOR136-1 and its $D109A^{3.37}$ mutant, we speculate that the wild-type aspartate residue causes dynamic partial occlusion of the ketamine-binding site, which is responsible for the intermediate ketamine responsiveness, relative to receptorswith smaller residues (high ketamine responsiveness) and larger residues (low ketamine responsiveness) at position $109^{3.37}$. We further tested this idea by calculating cavity volume using the computed atlas of surface topography of proteins (CASTp) software (45) with a 1.4-Å radius probe. The solvent-accessible cavity volume of the putative binding pocket decreased from 896 $\text{Å}^3$ in the wild-type MOR136-1 to 471 $\text{Å}^3$ in the $D109K^{3.37}$ mutant. A Lys at this position (fig. S5B) effectively divided the cavity into two smaller volumes, neither of which could accommodate ketamine. However, the cavity volume is essentially unchanged in the MOR136-1 $D109A^{3.37}$ mutant relative to that in the wild-type receptor model (table S3), indicating that volumes calculated from static model structures do not have the fidelity to resolve the differences in ketamine responsiveness between the wild-type and $D109A^{3.37}$ MOR136-1 receptors. These observations are consistent with the more dynamic nature of the ketamine-binding site occlusion by larger side chains, as suggested in the MD simulations.

Position $104^{3.32}$ was found to be of importance, in that the nonresponder MOR136-4 was converted to a responder by introducing the mutation $Y104F^{3.32}$. This position is located at the extracellular entry to the binding pocket (Fig. 2B and fig. S8), suggesting a gating mechanism. However, the MD simulations of MOR136-4 and its $Y104F^{3.32}$ mutant suggest that a hydrogen bond between the side chain of positions $Tyr104^{3.32}$ and $Thr279^{7.42}$ restricts the conformational freedom of $Tyr104^{3.32}$, thereby sterically altering the ketamine-binding site (fig. S8A). It is also possible that the lack of responsiveness relates to an inability of $Thr279^{7.42}$ on TM7 to interact with the ketamine Cl atom, because $Thr279^{7.42}$ is instead hydrogen-bonded to $Tyr104^{3.32}$ (Fig. 2D and fig. S3B). CASTp (45) calculations indicate a

large gain of pocket volume in the Y104F$^{3.32}$ MOR136-4 mutant (table S3), suggesting a steric rather than electrostatic mechanism (fig. S8D). We note that the presence of Tyr104$^{3.32}$ may not entirely impede ketamine activation of the receptor, because the single mutation N112S$^{3.40}$, which introduces the previously identified Ser112$^{3.40}$, confers some ketamine responsiveness to MOR136-4 (Table 2 and Fig. 4). Indeed, ignoring shape, the pocket volume of the wild-type receptor (Y104$^{3.32}$) should be adequate to accommodate ketamine.

At this time, there are no reported high-resolution structures of ORs; therefore, our structural analyses necessarily use comparative OR homology models, which are based on previously published structures of other GPCRs (see Materials and Methods) (20–24). The broad tertiary structures of GPCRs are reliably recovered through comparative modeling, but the models still might not capture structural details that substantially affect ketamine binding. Nevertheless, the degree of success with which our predicted mutations were able to modulate ketamine responsiveness in either direction suggests that such models can indeed be useful. Another limitation is that the structures used all correspond to an inactive state of the corresponding GPCR. One would anticipate that the use of structures of the active state would yield better results for an activating ligand. We attempted to determine the magnitude of this limitation by comparing the structures of inactive and active structures (fig. S2). From the RMSD analysis of the backbone atoms that formed the seven TM helices and the adjacent perpendicular helix (TM1-TM7-H8), the difference between the inactive and active models is 2.3 Å, similar to the RMSD calculated for the inactive and active crystal structures of the $\beta_2$AR (2.5 Å) (21, 32). Furthermore, for the 16 positions that formed the ketamine-binding pocket, the backbone RMSD is only 1.6 Å, which was substantiated by the similarity in the ketamine-binding poses identified in each case. These small structural variations make it difficult to rigorously compare the differences in structures; thus, the experimental functional studies presented herein provide the more critical assessment of the models and our molecular understanding of ketamine binding and response in ORs. In future studies, it will be of interest to consider additional template structures, particularly the active structure of opsin, because it has been suggested as a promising template for modeling OR structures (46).

Finally, we observed the in vivo activation of OSNs labeled with a MOR136-1 cRNA probe after topical exposure to ketamine in a dose-dependent fashion, up to 25% with 300 μM ketamine. Because there are no available transgenic mouse strains with labeled MOR136-1–expressing OSNs, we identified these OSNs by FISH with cRNA probes transcribed from full-length MOR136-1, which could cross-hybridize with other MOR136 family member ORs because of sequence similarity. These other OR family members include ketamine-unresponsive ORs, which likely explains why only 25% of the labeled OSNs were activated by a high ketamine concentration.

In summary, we provide evidence for the highly specific and selective activation of discrete ORs by ketamine, which at least suggests that GPCRs could serve as functional targets of this general anesthetic, but also suggests that CNS ORs could be targets of anesthetics or psychotropic drugs. Furthermore, through a combination of molecular modeling, sequence comparison, and mutagenesis, we characterized the important structural determinants of

ketamine activation by both removing and introducing responsiveness in specific receptors. The optimized combination of spatial key interaction loci in the binding pocket for ketamine could potentially be used as a signature binding pocket to search protein structural databases for other candidate ketamine receptors.

# MATERIALS AND METHODS

## In vitro luciferase activity assays to measure OR activation

In vitro assays to determine OR activation were performed as previously detailed (16, 17). Briefly, Hana3A cells were cotransfected with pCI plasmids encoding ORs containing an N-terminal rhodopsin tag (labeled Rho-pCI) together with luciferase reporter plasmids and plasmids encoding the cofactors receptor transport protein 1 (RTP1) and muscarinic acetylcholine receptor $M_3$, which enhance the functional expression of OR. Twenty-four hours after transfection, rich culture medium was replaced with CD293 chemically defined medium containing the appropriate concentrations of the desired anesthetics for 4 hours, after which the cells were lysed and luminescence was measured with the Dual-Glo Luciferase Assay System (Promega) with a POLARstar OPTIMA microplate reader (BMG Labtech). A minimum of three experiments with at least three technical replicates were performed for each OR-anesthetic pairing and at each concentration.

## Data analysis of luciferase activity measurement

Luciferase data values were normalized for transfection efficiency, plate-to-plate variation, and baseline-subtracted with solvent-only responses, and then were normalized to the maximal MOR136-1 responses obtained from the dose-response curve fits, which are set to 1.0. Data analysis, nonlinear regression, and statistical tests were performed with GraphPad Prism v5 software. Statistical significance was determined by ANOVA (analysis of variance) analysis with Bonferroni posttests at $P$    0.05 for comparisons at a single anesthetic concentration (Fig. 1A). Nonlinear regression curves were fitted for dose-response experiments, and $EC_{50}$ values are shown for curve fits with $R^2$    0.95. Fitted $EC_{50}$ values were compared pairwise by an extra sum-of-squares $F$ test at a significance level of $P < 0.05$. A minimum of three experiments with at least three technical replicates were performed for each analysis.

## Cell surface receptor expression studies

The cell surface expression of ORs was determined by FACS analysis. HEK 293 T cells were transfected with plasmids encoding N-terminal rhodopsin–tagged ORs or vector only control (Rho-pCI) and the same cofactors used in our in vitro luciferase assays, together with plasmid encoding green fluorescent protein (GFP), to monitor transfection efficiency. Live cells were stained with mouse anti-rhodopsin monoclonal antibody 4D2 [a gift from R. Molday (47)] followed by phycoerythrin (PE)–conjugated anti-mouse immunoglobulin G (Jackson Immunologicals), together with 7-aminoactinomycin D (7AAD, Calbiochem), to mark dead cells, which were excluded from analysis. FACS analysis was performed with FlowJo v10 software. Ten thousand GFP-positive (transfected), 7AAD-negative (live) cells were counted for each OR, cell counts were plotted in histograms using PE intensity (surface

staining intensity), and the population geometric mean fluorescence intensity was calculated as a measure of surface expression.

## Site-directed mutagenesis

Site-directed mutagenesis was performed by a two-step polymerase chain reaction (PCR) method essentially as previously described (48). For each of the mutants, primers for the full-length OR and mutually complementary mutagenesis primers containing mismatching bases for the mutated codons (table S4, altered bases are shown in lower case) were used to generate 5′ and 3′ fragments of the OR with overlapping ends containing the desired mutation. These fragments were purified and combined in a second PCR with only the respective full-length OR primers to generate a full-length OR containing the desired mutations, which were verified by Sanger sequencing.

## Comparative homology modeling

The amino acid sequences of MOR136-1 (Q8VGL0), the human $\beta_2AR$ (P07550), the bovine rhodopsin (P02699), the turkey $\beta_1AR$ (P07700), the human $A_{2A}$ adenosine receptor (P29274), and the human $D_3$ dopamine receptor (P35462) were obtained from the UniProt Knowledgebase (49). The pairwise sequence alignment between MOR136-1 and the human $\beta_2AR$ was performed with Blastp software (50) using the BLOSUM62 substitution matrix (51). Similar pairwise alignments between MOR136-1 and the other four templates were performed. Highly conserved fingerprint residues from the rhodopsin-like GPCR family were used to guide the final sequence alignment (52). Previous studies of ORs also guided the final multiple alignment (30, 36–39). Similar procedures were used during generation of the structures of the other ORs considered in this work. From the final sequence alignment (fig. S1), 100 structures of each of the ORs were constructed with the Modeller 9v8 software (25, 26), with the refinement optimization level adjusted to slow (25, 26). Modeller extracts different structural restraints in the form of probability distribution functions for structural features from the set of three-dimensional structures of the templates and then optimizes these restraints to generate the structures of a target sequence. The structures of the five GPCRs were used as templates in the generation of the different OR models. For each of the OR sequences, the best structure according to the scoring function used in Modeller was selected for subsequent modeling.

## Docking calculations

The structure of R-ketamine (CID: 3821) was obtained from the PubChem substance and compound database (53). The structure of camphor was obtained from the Protein Data Bank (PDB) [PDB accession 1IWJ (54)]. The docking calculations were performed with the AutoDock4 program (34). The geometry of the ligands was optimized with the semiempirical method PM3 using MOPAC2009 (55). The semiempirical method was also used to calculate the partial charges. During the docking calculations, the Lamarckian genetic algorithm was used with an optimized local search method (56). For the ligands, the initial position, orientation, and value of the torsion angles were randomly selected.

## Sequence comparison

Thirteen sequences in the MOR136 family (MOR136-1 to MOR136-13) considered in the experimental screens were obtained from the UniProt Knowledgebase (49). A multiple-sequence alignment was performed with ClustalW2, and the rendering of the alignment was prepared using SeaView (fig. S4). An alignment of the 16 positions in the putative binding pocket (positions: Phe73[2.53], Phe104[3.32], Ser105[3.33], Ala108[3.36], Asp109[3.37], Glu111[3.39], Ser112[3.40], Leu202[5.42], Gly203[5.43], Val206[5.46], Ile207[5.47], Tyr251[6.44], Ile255[6.48], Leu258[6.51], Tyr259[6.52], and Thr279[7.42] in MOR136-1) of the responders and nonresponders (MOR136-2, MOR136-4, and MOR136-6 to MOR136-13) was generated.

## Constrained MD simulations

To obtain statistics about conformations explored by the side chains of residues in the putative ketamine-binding site, all-atom MD simulations were performed on the model of MOR136-1 obtained by comparative modeling. The simulations were performed with NAMD2 (57) and the CHARMM22 force field (58) without the presence of ketamine. No lipid membrane was included, and the C$\alpha$ carbon atoms were fixed to their original positions. Water molecules (TIP3P model) (59) and ions (Na$^+$ and Cl$^-$) (58) were included in the simulations. The constrained MD simulation of the entire system was performed in the NPTensemble. Langevin dynamics and the hybrid Nosé-Hoover Langevin piston were used to maintain constant temperature (310 K) and constant pressure (1 atm), respectively (60). Electrostatic interactions were evaluated with the particle mesh Ewald technique with a grid spacing less than 1.0 Å for each dimension and a fourth-order interpolation (61). A time step of 1 fs was used for the simulations. Periodic boundary conditions were used with a periodic cell of 74 Å × 95 Å × 62 Å. A similar protocol was used in the case of the MOR136-1 mutant D109A[3.37], wild-type MOR136-4, and MOR136-4 mutant Y104F[3.32]. About 100-ns simulations were performed in all cases with a time step of 1.0 fs.

## In vivo OSN activation assay

Mice were anesthetized with isoflurane in 100% oxygen for 4.5 min. While immobilized, the mice were injected intranasally with 50 μl of 3, 30, or 300 μM ketamine in PBS, along with a PBS-only control, with a blunt syringe. The mice were allowed to recover for 1 hour and then were euthanized by $CO_2$ asphyxiation. Their nasal epithelia were harvested, frozen, and cryosectioned at 20-μm thickness. Detection of OR expression was performed by FISH of full-length, digoxigenin-labeled cRNA probes of MOR136-1 and M71 essentially as described previously (62), which was followed by antibody staining of pS6 (Cell Signaling antibody #2215) and Hoechst (bisBenzimide, Sigma B2883) to label nuclei.

# Supplementary Material

Refer to Web version on PubMed Central for supplementary material.

# Acknowledgments

## REFERENCES AND NOTES

1. Franks NP. General anaesthesia: From molecular targets to neuronal pathways of sleep and arousal. Nat. Rev. Neurosci. 2008; 9:370–386. [PubMed: 18425091]

2. Rasmussen KG, Lineberry TW, Galardy CW, Kung S, Lapid MI, Palmer BA, Ritter MJ, Schak KM, Sola CL, Hanson AJ, Frye MA. Serial infusions of low-dose ketamine for major depression. J. Psychopharmacol. 2013; 27:444–450. [PubMed: 23428794]

3. Nickols HH, Conn PJ. Development of allosteric modulators of GPCRs for treatment of CNS disorders. Neurobiol. Dis. 2014; 61:55–71. [PubMed: 24076101]

4. Urs NM, Nicholls PJ, Caron MG. Integrated approaches to understanding antipsychotic drug action at GPCRs. Curr. Opin. Cell Biol. 2014; 27:56–62. [PubMed: 24680431]

5. Thompson MD, Burnham WM, Cole DE. The G protein-coupled receptors: Pharmacogenetics and disease. Crit. Rev. Clin. Lab. Sci. 2005; 42:311–392. [PubMed: 16281738]

6. Minami K, Uezono Y. The recent progress in research on effects of anesthetics and analgesics on G protein-coupled receptors. J. Anesth. 2013; 27:284–292. [PubMed: 23099434]

7. Ishizawa Y, Sharp R, Liebman PA, Eckenhoff RG. Halothane binding to a G protein coupled receptor in retinal membranes by photoaffinity labeling. Biochemistry. 2000; 39:8497–8502. [PubMed: 10913255]

8. Buck L, Axel R. A novel multigene family may encode odorant receptors: A molecular basis for odor recognition. Cell. 1991; 65:175–187. [PubMed: 1840504]

9. Malnic B, Hirono J, Sato T, Buck LB. Combinatorial receptor codes for odors. Cell. 1999; 96:713–723. [PubMed: 10089886]

10. Bushdid C, Magnasco MO, Vosshall LB, Keller A. Humans can discriminate more than 1 trillion olfactory stimuli. Science. 2014; 343:1370–1372. [PubMed: 24653035]

11. Peterlin Z, Ishizawa Y, Araneda R, Eckenhoff R, Firestein S. Selective activation of G-protein coupled receptors by volatile anesthetics. Mol. Cell. Neurosci. 2005; 30:506–512. [PubMed: 16185894]

12. Flegel C, Manteniotis S, Osthold S, Hatt H, Gisselmann G. Expression profile of ectopic olfactory receptors determined by deep sequencing. PLOS One. 2013; 8:e55368. [PubMed: 23405139]

13. Pluznick JL, Protzko RJ, Gevorgyan H, Peterlin Z, Sipos A, Han J, Brunet I, Wan LX, Rey F, Wang T, Firestein SJ, Yanagisawa M, Gordon JI, Eichmann A, Peti-Peterdi J, Caplan MJ. Olfactory receptor responding to gut microbiota-derived signals plays a role in renin secretion and blood pressure regulation. Proc. Natl. Acad. Sci. U.S.A. 2013; 110:4410–4415. [PubMed: 23401498]

14. Fukuda N, Yomogida K, Okabe M, Touhara K. Functional characterization of a mouse testicular olfactory receptor and its role in chemosensing and in regulation of sperm motility. J. Cell Sci. 2004; 117:5835–5845. [PubMed: 15522887]

15. Spehr M, Gisselmann G, Poplawski A, Riffell JA, Wetzel CH, Zimmer RK, Hatt H. Identification of a testicular odorant receptor mediating human sperm chemotaxis. Science. 2003; 299:2054–2058. [PubMed: 12663925]

16. Saito H, Chi Q, Zhuang H, Matsunami H, Mainland JD. Odor coding by a mammalian receptor repertoire. Sci. Signal. 2009; 2:ra9. [PubMed: 19261596]

17. Zhuang H, Matsunami H. Evaluating cell-surface expression and measuring activation of mammalian odorant receptors in heterologous cells. Nat. Protoc. 2008; 3:1402–1413. [PubMed: 18772867]

18. White PF, Schüttler J, Shafer A, Stanski DR, Horai Y, Trevor AJ. Comparative pharmacology of the ketamine isomers: Studies in volunteers. Br. J. Anaesth. 1985; 57:197–203. [PubMed: 3970799]

19. Kufareva I, Katritch V, G. D. Participants of. Stevens RC, Abagyan R. Advances in GPCR modeling evaluated by the GPCR Dock 2013 assessment: Meeting new challenges. Structure. 2014; 22:1120–1139. [PubMed: 25066135]

20. Okada T, Sugihara M, Bondar AN, Elstner M, Entel P, Buss V. The retinal conformation and its environment in rhodopsin in light of a new 2.2 Å crystal structure. J. Mol. Biol. 2004; 342:571–583. [PubMed: 15327956]

21. Cherezov V, Rosenbaum DM, Hanson MA, Rasmussen SG, Thian FS, Kobilka TS, Choi HJ, Kuhn P, Weis WI, Kobilka BK, Stevens RC. High-resolution crystal structure of an engineered human β2-adrenergic G protein–coupled receptor. Science. 2007; 318:1258–1265. [PubMed: 17962520]

22. Warne T, Serrano-Vega MJ, Baker JG, Moukhametzianov R, Edwards PC, Henderson R, Leslie AG, Tate CG, Schertler GF. Structure of a β1-adrenergic G-protein-coupled receptor. Nature. 2008; 454:486–491. [PubMed: 18594507]

23. Jaakola VP, Griffith MT, Hanson MA, Cherezov V, Chien EY, Lane JR, Ijzerman AP, Stevens RC. The 2.6 angstrom crystal structure of a human A2A adenosine receptor bound to an antagonist. Science. 2008; 322:1211–1217. [PubMed: 18832607]

24. Chien EY, Liu W, Zhao Q, Katritch V, Han GW, Hanson MA, Shi L, Newman AH, Javitch JA, Cherezov V, Stevens RC. Structure of the human dopamine D3 receptor in complex with a D2/D3 selective antagonist. Science. 2010; 330:1091–1095. [PubMed: 21097933]

25. Sali A, Blundell TL. Comparative protein modeling by satisfaction of spatial restraints. J. Mol. Biol. 1993; 234:779–815. [PubMed: 8254673]

26. Eswar N, Webb B, Marti-Renom MA, Madhusudhan MS, Eramian D, Shen M-Y, Pieper U, Sali A. Comparative protein structure modeling using MODELLER. Curr. Protoc. Protein Sci. 2007 Chapter 2, Unit 2.9.

27. Pierce KL, Premont RT, Lefkowitz RJ. Seven-transmembrane receptors. Nat. Rev. Mol. Cell Biol. 2002; 3:639–650. [PubMed: 12209124]

28. Hanson MA, Stevens RC. Discovery of new GPCR biology: One receptor structure at a time. Structure. 2009; 17:8–14. [PubMed: 19141277]

29. Rosenbaum DM, Rasmussen SG, Kobilka BK. The structure and function of G-protein-coupled receptors. Nature. 2009; 459:356–363. [PubMed: 19458711]

30. Man O, Gilad Y, Lancet D. Prediction of the odorant binding site of olfactory receptor proteins by human–mouse comparisons. Protein Sci. 2004; 13:240–254. [PubMed: 14691239]

31. Choe HW, Kim YJ, Park JH, Morizumi T, Pai EF, Krauss N, Hofmann KP, Scheerer P, Ernst OP. Crystal structure of metarhodopsin II. Nature. 2011; 471:651–655. [PubMed: 21389988]

32. Rasmussen SG, DeVree BT, Zou Y, Kruse AC, Chung KY, Kobilka TS, Thian FS, Chae PS, Pardon E, Calinski D, Mathiesen JM, Shah ST, Lyons JA, Caffrey M, Gellman SH, Steyaert J, Skiniotis G, Weis WI, Sunahara RK, Kobilka BK. Crystal structure of the β2 adrenergic receptor–Gs protein complex. Nature. 2011; 477:549–555. [PubMed: 21772288]

33. Rasmussen SG, Choi HJ, Fung JJ, Pardon E, Casarosa P, Chae PS, Devree BT, Rosenbaum DM, Thian FS, Kobilka TS, Schnapp A, Konetzki I, Sunahara RK, Gellman SH, Pautsch A, Steyaert J, Weis WI, Kobilka BK. Structure of a nanobody-stabilized active state of the β2 adrenoceptor. Nature. 2011; 469:175–180. [PubMed: 21228869]

34. Morris GM, Huey R, Lindstrom W, Sanner MF, Belew RK, Goodsell DS, Olson AJ. AutoDock4 and AutoDockTools4: Automated docking with selective receptor flexibility. J. Comput. Chem. 2009; 30:2785–2791. [PubMed: 19399780]

35. Ballesteros JA, Weinstein H. Integrated methods for the construction of three-dimensional models and computational probing of structure-function relations in G protein-coupled receptors. Methods Neurosci. 1995; 25:366–428.

36. Baud O, Etter S, Spreafico M, Bordoli L, Schwede T, Vogel H, Pick H. The mouse eugenol odorant receptor: Structural and functional plasticity of a broadly tuned odorant binding pocket. Biochemistry. 2011; 50:843–853. [PubMed: 21142015]

37. Katada S, Hirokawa T, Oka Y, Suwa M, Touhara K. Structural basis for a broad but selective ligand spectrum of a mouse olfactory receptor: Mapping the odorant-binding site. J. Neurosci. 2005; 25:1806–1815. [PubMed: 15716417]

38. Abaffy T, Malhotra A, Luetje CW. The molecular basis for ligand specificity in a mouse olfactory receptor: A network of functionally important residues. J. Biol. Chem. 2007; 282:1216–1224. [PubMed: 17114180]

39. Schmiedeberg K, Shirokova E, Weber H-P, Schilling B, Meyerhof W, Krautwurst D. Structural determinants of odorant recognition by the human olfactory receptors OR1A1 and OR1A2. J. Struct. Biol. 2007; 159:400–412. [PubMed: 17601748]

40. Venkatakrishnan AJ, Deupi X, Lebon G, Tate CG, Schertler GF, Babu MM. Molecular signatures of G-protein-coupled receptors. Nature. 2013; 494:185–194. [PubMed: 23407534]

41. Cao R, Lee B, Cho HY, Saklayen S, Obrietan K. Photic regulation of the mTOR signaling pathway in the suprachiasmatic circadian clock. Mol. Cell. Neurosci. 2008; 38:312–324. [PubMed: 18468454]

42. Knight ZA, Tan K, Birsoy K, Schmidt S, Garrison JL, Wysocki RW, Emiliano A, Ekstrand MI, Friedman JM. Molecular profiling of activated neurons by phosphorylated ribosome capture. Cell. 2012; 151:1126–1137. [PubMed: 23178128]

43. Valjent E, Bertran-Gonzalez J, Bowling H, Lopez S, Santini E, Matamales M, Bonito-Oliva A, Hervé D, Hoeffer C, Klann E, Girault JA, Fisone G. Haloperidol regulates the state of phosphorylation of ribosomal protein S6 via activation of PKA and phosphorylation of DARPP-32. Neuropsychopharmacology. 2011; 36:2561–2570. [PubMed: 21814187]

44. Feldmesser E, Olender T, Khen M, Yanai I, Ophir R, Lancet D. Widespread ectopic expression of olfactory receptor genes. BMC Genomics. 2006; 7:121. [PubMed: 16716209]

45. Dundas J, Ouyang Z, Tseng J, Binkowski A, Turpaz Y, Liang J. CASTp: Computed atlas of surface topography of proteins with structural and topographical mapping of functionally annotated residues. Nucleic Acids Res. 2006; 34:W116–W118. [PubMed: 16844972]

46. Park JH, Morizumi T, Li Y, Hong JE, Pai EF, Hofmann KP, Choe HW, Ernst OP. Opsin, a structural model for olfactory receptors? Angew. Chem. Int. Ed. Engl. 2013; 52:11021–11024. [PubMed: 24038729]

47. Laird DW, Molday RS. Evidence against the role of rhodopsin in rod outer segment binding to RPE cells. Invest. Ophthalmol. Vis. Sci. 1988; 29:419–428. [PubMed: 3343097]

48. Ho SN, Hunt HD, Horton RM, Pullen JK, Pease LR. Site-directed mutagenesis by overlap extension using the polymerase chain reaction. Gene. 1989; 77:51–59. [PubMed: 2744487]

49. Jain E, Bairoch A, Duvaud S, Phan I, Redaschi N, Suzek BE, Martin MJ, McGarvey P, Gasteiger E. Infrastructure for the life sciences: Design and implementation of the UniProt website. BMC Bioinformatics. 2009; 10:136. [PubMed: 19426475]

50. Altschul SF, Gish W, Miller W, Myers EW, Lipman DJ. Basic local alignment search tool. J. Mol. Biol. 1990; 215:403–410. [PubMed: 2231712]

51. Henikoff S, Henikoff JG. Amino acid substitution matrices from protein blocks. Proc. Natl. Acad. Sci. U.S.A. 1992; 89:10915–10919. [PubMed: 1438297]

52. Surratt CK, Adams WR. G protein-coupled receptor structural motifs: Relevance to the opioid receptors. Curr. Top. Med. Chem. 2005; 5:315–324. [PubMed: 15857314]

53. Bolton E, Wang Y, Thiessen PA, Bryant SH. PubChem: Integrated platform of small molecules and biological activities. Annu. Rep. Comput. Chem. 2008; 4:217–241.

54. Nagano S, Shimada H, Tarumi A, Hishiki T, Kimata-Ariga Y, Egawa T, Suematsu M, Park SY, Adachi S, Shiro Y, Ishimura Y. Infrared spectroscopic and mutational studies on putidaredoxin-induced conformational changes in ferrous CO-P450cam. Biochemistry. 2003; 42:14507–14514. [PubMed: 14661963]

55. Stewart, JJP. MOPAC2009. Stewart Computational Chemistry, Colorado Springs, CO; 2008. OpenMOPAC.net

56. Solis FJ, Wets RJ-B. Minimization by random search techniques. Math. Oper. Res. 1981; 6:19–30.

57. Phillips JC, Braun R, Wang W, Gumbart J, Tajkhorshid E, Villa E, Chipot C, Skeel RD, Kalé L, Schulten K. Scalable molecular dynamics with NAMD. J. Comput. Chem. 2005; 26:1781–1802. [PubMed: 16222654]

58. MacKerell AD, Bashford D, Bellott M, Dunbrack RL, Evanseck JD, Field MJ, Fischer S, Gao J, Guo H, Ha S, Joseph-McCarthy D, Kuchnir L, Kuczera K, Lau FTK, Mattos C, Michnick S, Ngo T, Nguyen DT, Prodhom B, Reiher WE, Roux B, Schlenkrich M, Smith JC, Stote R, Straub J, Watanabe M, Wiórkiewicz-Kuczera J, Yin D, Karplus M. All-atom empirical potential for molecular modeling and dynamics studies of proteins. J. Phys. Chem. B. 1998; 102:3586–3616. [PubMed: 24889800]

59. Jorgensen WL, Chandrasekhar J, Madura JD, Impey RW, Klein ML. Comparison of simple potential functions for simulating liquid water. J. Chem. Phys. 1983; 79:926–935.

60. Feller SE, Zhang YH, Pastor RW, Brooks BR. Constant pressure molecular dynamics simulation: The Langevin piston method. J. Chem. Phys. 1995; 103:4613–4621.

61. Darden T, York D, Pedersen L. Particle mesh Ewald: An $N{\cdot}\log(N)$ method for Ewald sums in large systems. J. Chem. Phys. 1993; 98:10089–10092.

62. Davidson LA, Keller RE. Neural tube closure in *Xenopus laevis* involves medial migration, directed protrusive activity, cell intercalation and convergent extension. Development. 1999; 126:4547–4556. [PubMed: 10498689]
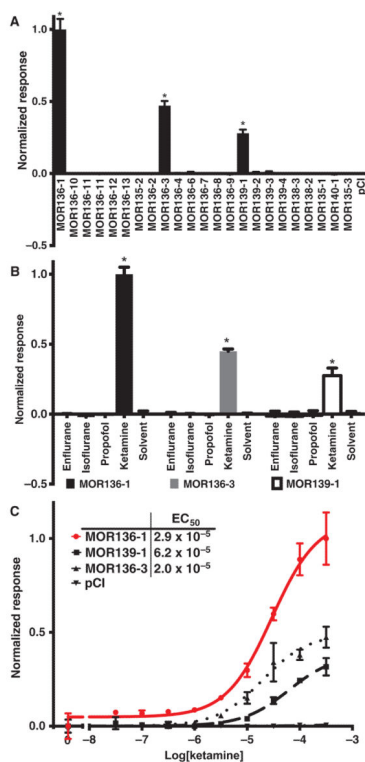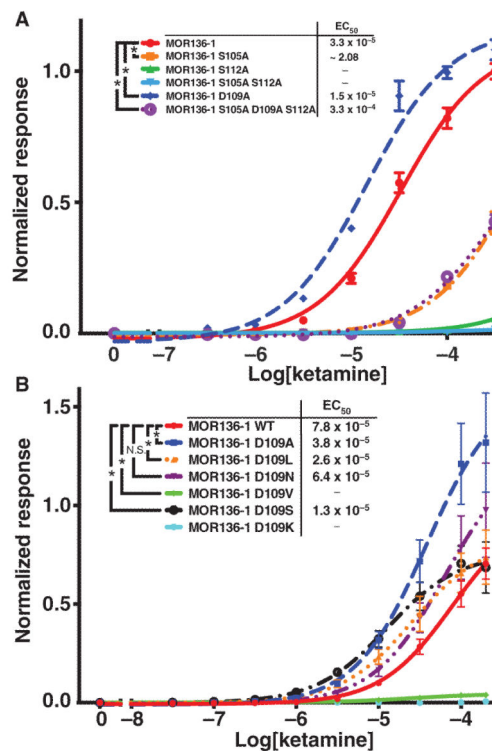
**Fig. 1. MOR136-1, MOR136-3, and MOR139-1 respond specifically to ketamine**

(**A**) Hana3A cells cotransfected with a luciferase reporter plasmid and plasmids encoding the indicated ORs or pCI as a negative control were treated with 100 μM ketamine for 4 hours, and then were analyzed by luciferase assay to determine receptor responsiveness. Luciferase activity was normalized to that of cells expressing MOR136-1, which was set at 1.0. Data are means ± SEM of three independent experiments. (**B**) In a separate experiment, Hana3A cells cotransfected with a luciferase reporter plasmid and plasmids encoding MOR136-1, MOR136-3, or MOR139-1 were treated with the indicated anesthetics (each at 100 μM) or with solvent (negative control) for 4 hours, and then were analyzed by luciferase assay to determine receptor responsiveness. Luciferase activity was normalized to that of ketamine-treated cells expressing MOR136-1, which was set at 1.0. Data are means ± SEM of three independent experiments. (**C**) Hana3A cells cotransfected with a luciferase reporter plasmid and plasmids encoding MOR136-1, MOR136-3, or MOR139-1, as indicated, or with pCI as a negative control were treated with the indicated concentrations of ketamine for 4 hours, and then were analyzed by luciferase assay to determine receptor responsiveness. Luciferase activity was normalized to the fitted maximum response of cells expressing MOR136-1, which was set at 1.0. The respective $EC_{50}$ values for each of the receptors are indicated. Data are means ± SEM of three independent experiments.
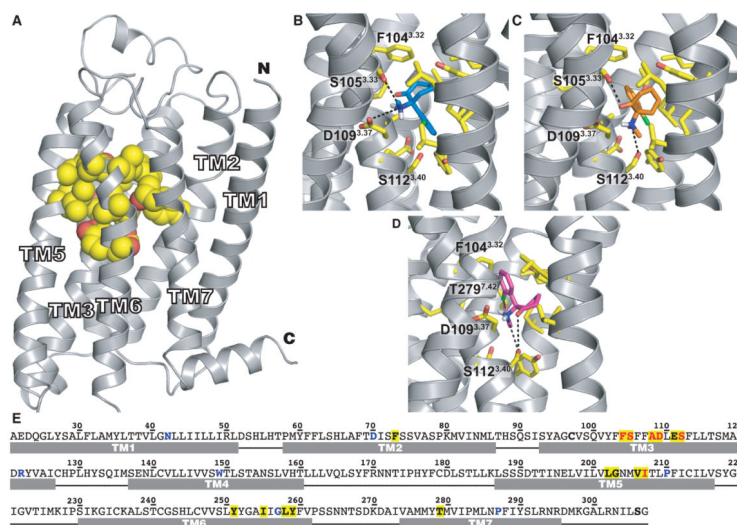
**Fig. 2. The model structure and ketamine-docking poses of MOR136-1**

(**A**) The MOR136-1 model structure was obtained by comparative modeling. The 16 positions identified to form the ketamine-binding site (within 5.0 Å of docked ketamine molecules) are displayed as space-filling representations (yellow). Residues forming the ketamine-binding pocket are located mainly in TM3, TM5, and TM6, with just one residue in TM2 and one in TM7. (**B**) Pose 1 of ketamine (blue) in MOR136-1 obtained from the docking calculation. Possible interactions of the positively charged nitrogen of ketamine with Ser105$^{3.33}$ and Asp109$^{3.37}$ are indicated. (**C**) Pose 2 of ketamine (orange) in MOR136-1 shows the interactions of the positively charged nitrogen of ketamine with Ser112$^{3.40}$ and the keto moiety with Ser105$^{3.33}$. (**D**) The ketamine pose 3 (magenta) from docking calculations indicates not only an interaction between the nitrogen in ketamine and Ser112$^{3.40}$ but also a possible interaction of the Cl atom with residue Thr279$^{7.42}$. (**E**) Complete sequence of MOR136-1. The 16 positions predicted to form the putative ketamine-binding site are highlighted in yellow. The conserved residues (conserved in class A GPCRs) at each of the TM helices are colored in blue. The six positions considered in the mutagenesis studies are colored in red.

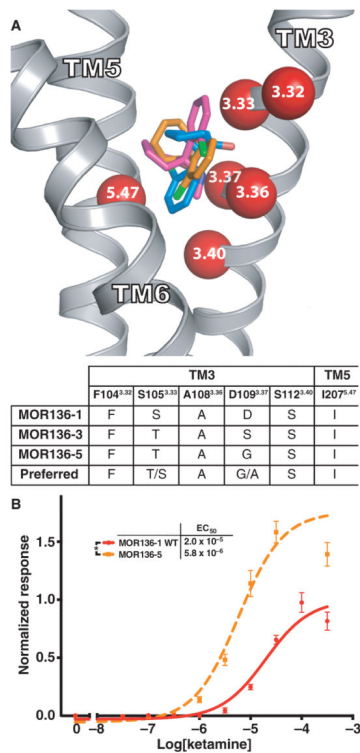**Fig. 3. Dose-response curves for mutant MOR136-1 receptors**

(**A**) Hana3A cells cotransfected with a luciferase reporter plasmid and plasmids encoding MOR136-1 and the S105A$^{3.33}$, S112A$^{3.40}$, S105A$^{3.33}$/S112A$^{3.40}$, D109A$^{3.37}$, and S105A$^{3.33}$/D109A$^{3.37}$/S112A$^{3.40}$ mutants, as indicated, or with pCI as a negative control were treated with the indicated concentrations of ketamine for 4 hours, and then were analyzed by luciferase assay to determine receptor responsiveness. Luciferase activity was normalized to the fitted maximum response of cells expressing MOR136-1, which was set at 1.0. The respective EC$_{50}$ values for each of the receptors are indicated. Data are means ± SEM of five independent experiments. (**B**) Hana3A cells cotransfected with a luciferase reporter plasmid and plasmids encoding MOR136-1 and the D109A$^{3.37}$, D109L$^{3.37}$, D109N$^{3.37}$, D109V$^{3.37}$, D109S$^{3.37}$, and D109K$^{3.37}$ mutants, as indicated, or with pCI as a negative control were treated with the indicated concentrations of ketamine for 4 hours, and then were analyzed by luciferase assay to determine receptor responsiveness. Luciferase activity was normalized to the fitted maximum response of cells expressing MOR136-1, which was set at 1.0. The respective EC$_{50}$ values for each of the receptors are indicated. Data are means ± SEM of eight independent experiments. N.S., not significant.
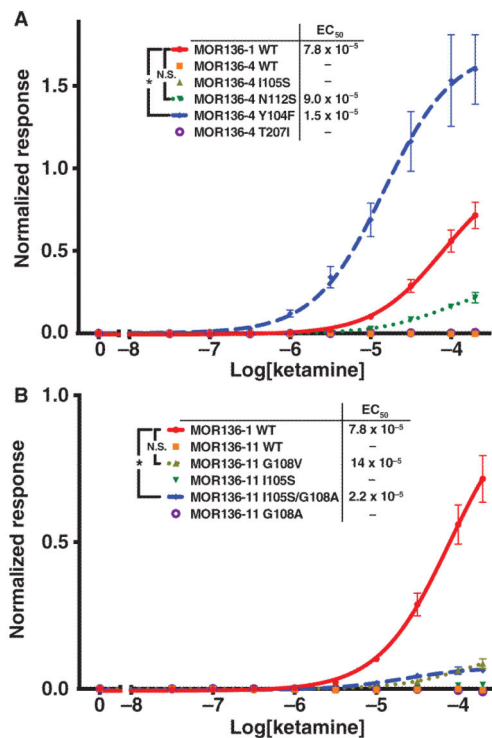
**Fig. 4. Dose-response curves for point mutants of MOR136-4 and MOR136-11**

(**A**) Hana3A cells cotransfected with a luciferase reporter plasmid and plasmids encoding MOR136-1, MOR136-4, or the MOR136-4 I105S[3.33], N112S[3.40], Y104F[3.32], and T207I[5.47] mutants, as indicated, or with pCI as a negative control were treated with the indicated concentrations of ketamine for 4 hours, and then were analyzed by luciferase assay to determine receptor responsiveness. Luciferase activity was normalized to the fitted maximum response of cells expressing MOR136-1, which was set at 1.0. The respective $EC_{50}$ values for each of the receptors are indicated. Data are means ± SEM of eight independent experiments. (**B**) Hana3A cells cotransfected with a luciferase reporter plasmid and plasmids encoding MOR136-1, MOR136-11, or the MOR136-11 G108V[3.36], I105S[3.33], I105S[3.33]/G108A[3.36], and G108A[3.36] mutants, as indicated, or with pCI as a negative control were treated with the indicated concentrations of ketamine for 4 hours, and then were analyzed by luciferase assay to determine receptor responsiveness. Luciferase activity was normalized to the fitted maximum response of cells expressing MOR136-1, which was set at 1.0. The respective $EC_{50}$ values for each of the receptors are indicated. Data are means ± SEM of eight independent experiments.

**Fig. 5. Representation of the ketamine-binding site and dose-response curves for MOR136-5**

(**A**) Top: Positions $104^{3.32}$, $105^{3.33}$, $108^{3.36}$, $109^{3.37}$, $112^{3.40}$, and $207^{5.47}$ (shown here as red spheres) were investigated by mutagenesis studies in the responder MOR136-1 and in the nonresponders MOR136-4 and MOR136-11. The three identified poses of ketamine are depicted as blue (pose 1), orange (pose 2), and magenta (pose 3) sticks, whereas the different TMs are shown as ribbons. Bottom: Summary of the investigated positions for the three wild-type (WT) ketamine responders: MOR136-1, MOR136-3, and MOR136-5. At each site, the "preferred" residue type for which the largest response was observed is also displayed. (**B**) Hana3A cells cotransfected with a luciferase reporter plasmid and plasmids encoding MOR136-1 or MOR136-5 were treated with the indicated concentrations of ketamine for 4 hours, and then were analyzed by luciferase assay to determine receptor responsiveness. Luciferase activity was normalized to the fitted maximum response of cells expressing MOR136-1, which was set at 1.0. The respective $EC_{50}$ values for each of the receptors are indicated. Data are means ± SEM of three independent experiments.
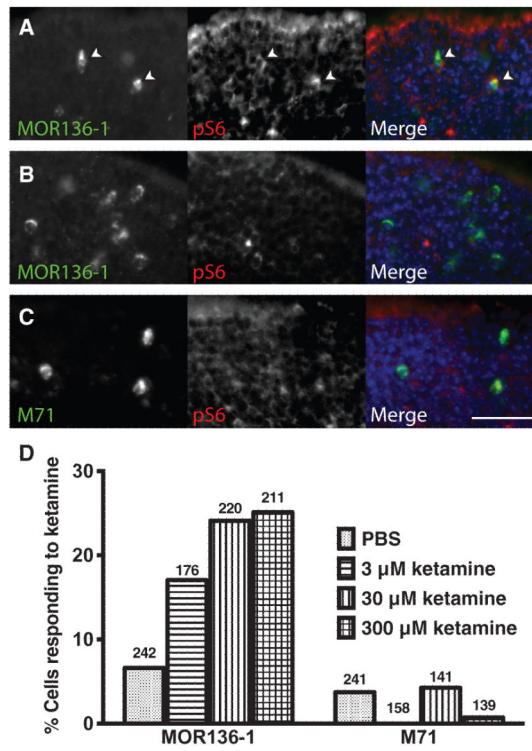
**Fig. 6. In vivo activation of OSNs by ketamine**

(**A** to **C**) C57BL/6J mice were lightly anesthetized with isoflurane and injected intranasally with 50 μl of ketamine (A and C) or PBS (B) as a negative control, and their nasal epithelia were harvested, frozen, cryosectioned, and stained as indicated. Scale bar, 50 μm. (**D**) OSNs that were treated with PBS or the indicated concentrations of ketamine were counted, and the percentage of the cells that had MOR136 family members (left) or M71 (right) and responded to ketamine was calculated. The total numbers of OSNs counted in each treatment condition are shown above the respective histogram bars.

## Table 1

**Sequence comparison of binding site residues for receptors in MOR136 family**

The three first receptors (MOR136-1, MOR136-3, and MOR136-5) in this family displayed responses to ketamine. Displayed are the 16 positions that were identified as ketamine-binding residues, where the first and second rows show the residue number of MOR136-1 and the Ballesteros-Weinstein (BW) numbering positions in the structure (35), respectively. The three natural responders only differ at position $109^{3.37}$ (green). For each of the nonresponders, the residue identities not present in any of the three responders at the corresponding position are indicated in red.

| Residue | 73 | 104 | 105 | 108 | 109 | 111 | 112 | 202 | 203 | 206 | 207 | 251 | 255 | 258 | 259 | 279 |
|---|---|---|---|---|---|---|---|---|---|---|---|---|---|---|---|---|
| BW position | 2.53 | 3.32 | 3.33 | 3.36 | 3.37 | 3.39 | 3.40 | 5.42 | 5.43 | 5.46 | 5.47 | 6.44 | 6.48 | 6.51 | 6.52 | 7.42 |
| **Responders** | | | | | | | | | | | | | | | | |
| MOR136-1 | F | F | S | A | D | E | S | L | G | V | I | Y | I | L | Y | T |
| MOR136-3 | F | F | T | A | S | D | S | L | G | V | I | Y | I | L | Y | T |
| MOR136-5 | F | F | T | A | G | D | S | L | G | V | I | Y | I | L | Y | T |
| **Non-responders** | | | | | | | | | | | | | | | | |
| MOR136-2 | F | F | S | T | D | D | S | L | G | V | I | Y | I | L | Y | S |
| MOR136-4 | F | Y | I | A | D | E | N | L | G | V | T | Y | I | L | Y | T |
| MOR136-6 | F | F | L | G | C | D | N | L | A | V | I | Y | I | L | Y | T |
| MOR136-7 | F | F | A | A | D | D | S | L | G | V | I | Y | I | L | Y | T |
| MOR136-8 | F | F | L | A | D | D | S | V | G | V | I | Y | I | L | Y | T |
| MOR136-9 | F | F | L | A | D | D | N | L | G | I | I | Y | I | L | Y | N |
| MOR136-10 | F | F | L | A | D | D | S | V | G | I | I | Y | I | L | Y | T |
| MOR136-11 | F | F | I | G | S | D | S | L | G | V | I | Y | V | L | Y | T |
| MOR136-12 | F | F | I | G | S | D | S | L | G | V | I | Y | I | L | Y | T |
| MOR136-13 | F | F | I | T | D | D | N | V | G | V | I | Y | I | V | Y | T |

**Table 2**

**Summary of the mutagenesis results involving the ketamine-responding receptor MOR136-1 and the nonresponders MOR136-4 and MOR136-11**

Except for the mutations at Asp109$^{3.37}$, the identified mutations led to a loss of responsiveness for MOR136-1. Identified mutations introduced responsiveness to the nonresponders MOR136-4 and MOR136-11 (see also Fig. 5A).

| | OR mutants and ketamine responses | | | |
|---|---|---|---|---|
| | Increased response | No effect | Decreased response | Eliminated response |
| **MOR136-1** | D109A$^{3.37}$ | D109L$^{3.37}$ | S105A$^{3.33}$ | F104Y$^{3.32}$ |
| | D109S$^{3.37}$ | D109N$^{3.37}$ | S105A$^{3.33}$/D109A$^{3.37}$/S112A$^{3.40}$ | S105A$^{3.33}$/S112A$^{3.40}$ |
| | | | | D109K$^{3.37}$ |
| | | | | D109V$^{3.37}$ |
| | | | | S112A$^{3.40}$ |
| **MOR136-4** | Y104F$^{3.32}$ | I105S$^{3.33}$ | — | — |
| | N112S$^{3.40}$ | T207I$^{5.47}$ | | |
| **MOR136-11** | I105S$^{3.33}$/G108A$^{3.36}$ | I105S$^{3.33}$ | — | — |
| | G108V$^{3.36}$ | *G108A$^{3.36}$ | | |

*The G108A$^{3.36}$ mutant of MOR136-11 was not expressed at the cell surface.